The Influence of Lamellar Orientation on Corneal Material Behavior: Biomechanical and Structural Changes in an Avian Corneal Disorder

Craig Boote,[1] *Ahmed Elsheikh,*[2] *Wael Kassem,*[2] *Christina S. Kamma-Lorger,*[1] *Paul M. Hocking,*[3] *Nick White,*[4] *Chris F. Inglehearn,*[5] *Manir Ali,*[5] *and Keith M. Meek*[1]

Purpose. Retinopathy, globe enlarged (RGE) is an inherited genetic disease of chickens with a corneal phenotype characterized by loss of tissue curvature and changes in peripheral collagen fibril alignment. This study aimed to characterize the material behavior of normal and RGE chicken corneas under inflation and compare this with new spatial- and depth-resolved microstructural information to investigate how stromal fibril architecture determines corneal behavior under intraocular pressure (IOP).

Methods. Six RGE chicken corneas and six age-matched normal controls were tested using trephinate inflation and their stress-strain behavior determined as a function of posterior pressure. Second harmonic generation mulitphoton microscopy was used to compare the in-plane appearance and degree of through-plane interlacing of collagen lamellae between normal and mutant corneas.

Results. RGE corneas displayed a 30–130% increase in material stiffness [$E_{tangent}$(RGE) = 0.94 ± 0.18 MPa to 3.09 ± 0.66 MPa; $E_{tangent}$(normals) = 0.72 ± 0.13 MPa to 1.34 ± 0.35 MPa] ($P \leq 0.05$). The normal in-plane disposition of anterior collagen in the peripheral cornea was altered in RGE but through-plane lamellar interlacing was unaffected.

Conclusions. This article demonstrates changes in corneal material behavior in RGE that are qualitatively consistent with microstructural collagen alterations identified both herein and previously. This study indicates that, in general, changes in stromal fibril orientation may significantly affect corneal material behavior and thereby its response to IOP. (*Invest Ophthalmol Vis Sci.* 2011;52:1243–1251) DOI:10.1167/iovs.10-5962

From the [1]Structural Biophysics Group and [4]Vision Science Bioimaging, School of Optometry and Vision Sciences, Cardiff University, Cardiff, United Kingdom; [2]Ocular Biomechanics Group, School of Engineering, University of Liverpool, Liverpool, United Kingdom; [3]Roslin Institute and Royal (Dick) School of Veterinary Studies, University of Edinburgh, Roslin BioCentre, Midlothian, United Kingdom; and [5]Leeds Institute of Molecular Medicine, University of Leeds, St. James's Hospital, Leeds, United Kingdom.

Supported by MRC Grants No. G0600755 and G0501050, The Wellcome Trust Grant No. 074165, and Biotechnology and Biological Sciences Research Council (BBSRC). KM is a Royal Society-Wolfson Research Merit Award holder.

Submitted for publication May 27, 2010; revised September 9, 2010; accepted October 2, 2010.

Disclosure: **C. Boote**, None; **A. Elsheikh**, None; **W. Kassem**, None; **C.S. Kamma-Lorger**, None; **P.M. Hocking**, None; **N. White**, None; **C.F. Inglehearn**, None; **M. Ali**, None; **K.M. Meek**, None

Corresponding author: Craig Boote, Structural Biophysics Group, School of Optometry and Vision Sciences, Cardiff University, Maindy Road, Cardiff CF24 4LU, UK; bootec@cf.ac.uk.

The cornea is the transparent component of the eye's outer layer. It provides a tough, protective envelope for the ocular contents and, in terrestrial vertebrates, also accounts for around two-thirds of the eye's refractive power.[1] The corneal stroma is formed by the superposition of several hundred individual lamellae that align roughly with the corneal surface, each comprising parallel, uniform-diameter collagen fibrils in a hydrated matrix.[2] However, the number, thickness, and preferential alignment of lamellae vary considerably between stromal depths and regions.[3] In addition, these same parameters show marked species-dependent differences, presumably driven by the need to balance diverse biomechanical prerequisites imposed by environment and behavior with the universal requirement for optical transparency.[4]

Corneal mechanical behavior is heavily influenced by stromal collagen architecture. Since collagen fibrils are strongest axially, lamellar anisotropy may be expected to confer direction dependency on the corneal elastic modulus,[5] as shown experimentally.[6–10] Allied to this, the degree of interaction between layers,[11] for example, via anterior-posterior lamellar interlacing,[12–14] may also impinge on the stroma's ability to support corneal tension.[15] From a clinical point of view, the stress-bearing ability of the cornea is likely to be important in determining the topography of the anterior corneal surface and its response to disease, refractive surgery, and changes in intraocular pressure (IOP).[16–18] However, to what degree, if any, collagen fibril organization influences the precise shape that the cornea adopts in response to a given IOP remains an open question.

Animal vision diseases in which normal eye development is compromised can provide valuable opportunities for investigating the relationship between corneal structure, mechanical behavior, and function. Retinopathy, globe enlarged (RGE) is an autosomal recessive disease of chickens,[19,20] arising from an in-frame 3-bp deletion in the cone β-transducin gene *GNB3*,[21] and is characterized clinically by progressive retinal degeneration and blindness by ~1 month posthatch.[22,23] Loss of functional vision triggers secondary globe enlargement and associated severe flattening of the cornea.[22,23] Previously we have shown using x-ray scattering that the development of misshapen corneas in RGE is accompanied by in-plane alterations in dominant peripheral collagen orientation.[24,25] We also used a numerical finite-element approach to demonstrate that these microstructural alterations are biomechanically consistent with changes in tissue stress predicted from the reshaping of the anterior globe.[25] However, a definitive link between microstructural, biomechanical, and morphometric corneal changes in RGE has not yet been established, in large part because the material properties of the RGE cornea have not been characterized. The present study was designed to provide this missing information by comparing the behavior of normal and RGE chicken corneas under varying simulated IOP, using trephinate

corneal inflation. In addition, second harmonic generation (SHG) multiphoton microscopy was used to compare the in-plane appearance of stromal lamellae, and their degree of through-plane interlacing, between normal and mutant tissue. Our overall aim was to gain qualitative experimental insight into the influence of collagen lamellar orientation on corneal behavior under IOP.

METHODS

Animal Details

Layer type White Leghorn chickens are maintained at the Roslin Institute (Edinburgh, UK). All husbandry and experimental techniques are performed under a Home Office project license in accordance with the ARVO statement for the Use of Animals in Ophthalmic and Vision Research. Birds are floor-reared with a daily photoperiod of 14 hours light (intensity, 20–30 lux) and 10 hours darkness, and transferred to individual cages at 16 weeks of age for pedigree breeding. The derivation and maintenance of the RGE line at Roslin has been described in detail by Inglehearn et al.[22]

Tissue Harvesting

Six homozygous (RGE/RGE) blind White Leghorn chickens and six normally sighted wild-type birds were euthanatized with an overdose of sodium pentabarbitone at 9 months old, an age at which the globe enlargement and corneal restructuring caused by the disease have proceeded to completion.[25] Immediately after death the eyes were enucleated and the posterior sclera punctured several times with a needle to aid perfusion of the preservation medium and minimize corneal swelling before the experiments. The right globes were then placed in silicon oil for subsequent inflation testing, and the left eyes were removed to 4% paraformaldehyde and stored at 4°C for microscopic assessment. The latter group also received a scleral suture to mark the superior corneal position.

Corneal Inflation Testing

Immediately before testing central (CCT) and peripheral (PCT) corneal thickness was measured via ultrasound pachymetry (DGH Pachmate 55; DGH Technologies, Exton, PA). The average values of CCT (±SD) were 334 ± 34 μm (normals) and 309 ± 15 μm (RGE). The corneas were then excised such that approximately 3 mm of the attached scleral rim was retained. Specimens were tested on a custom-developed corneal inflation rig designed to assess corneal deformation under simulated IOP (Fig. 1). A detailed description of this equipment may be found elsewhere.[26] In brief, it enables uninterrupted cycles of preselected pressure to be applied to the posterior cornea, while the deformation of the anterior surface is simultaneously measured. Specimens were connected along their rings of scleral tissue to the rig's pressure chamber using only mechanical clamps and without the need for adhesive, while allowing the cornea and limbus complete freedom to deform.

The pressure chamber was filled with a saline solution and connected to a reservoir whose height was computer controlled to set the applied pressure. Chamber pressure was recorded using an FDW-series pressure transducer (RDP Electronics, Wolverhampton, UK). Throughout the tests the saline solution in the pressure chamber was regulated at 37°C using a temperature controller and water bath (Fig. 1). The specimens' anterior surface was wetted regularly with a viscous tear film supplement (Visco-tears; Novartis, Sydney, Australia) to prevent drying. The wetting took place just before the start of each new pressure cycle and involved the release of three drops onto the clamping area above the cornea so that the tear film supplement would flow slowly over the specimen and maintain a thin film that would not interfere with the behavior-monitoring devices.

Non-contact behavior–monitoring devices were used throughout the test to record specimen deformation on pressure change. This included a 1 μm accuracy laser displacement sensor (LK-series; Keyence, Milton Keynes, UK), aligned normal to the corneal apex, and two digital cameras (FinePix S7000, 8 Mp; Fujifilm, Tokyo, Japan) positioned in the corneal plane to measure the initial corneal radius of curvature.

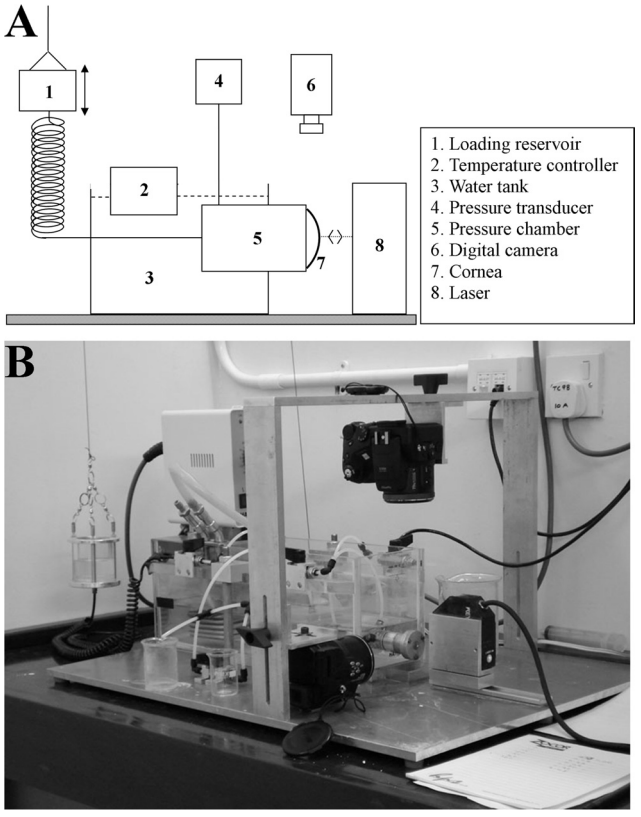

FIGURE 1. (**A**) Schematic showing main components of the corneal inflation rig. (**B**) Photograph of apparatus.

For each specimen three cycles of loading and unloading, up to a maximum pressure of 63 mm Hg (i.e., well above normal physiological levels), were applied to condition the tissue and stabilize its behavior before considering the results in a fourth cycle as representative of the cornea's biomechanical behavior. This is in line with previous studies in which corneal specimens demonstrated only small changes beyond the third loading cycle.[26–28] Sufficient recovery time (90 seconds) was allowed between loading cycles to ensure that the behavior remained unaffected by the strain history of preconditioning cycles.[29] The pressure change rate was set at 37.5 mm Hg/minutes by computer regulation of the loading reservoir's rate of vertical movement. This rate, which was the highest possible with the inflation rig, is comparable with the lower end of the scale of values expected during changes in posture.[30] Immediately after each test CCT and PCT were remeasured and found to be within 5% of the initial value for every specimen, indicating that corneal swelling due to the saline solution in the pressure chamber was minimal and could be ignored in the subsequent stress-strain calculations.

Mathematical shell analysis was used to derive the stress-strain behavior of each specimen from pressure-rise measurements recorded from the fourth loading cycle.[26] In brief, a geometrical representation was built for each cornea under an initial pressure of 0.75 mm Hg. The analysis approximated the cornea as a homogenous, spherical structure and considered the average limbal diameter and anterior radius of curvature (from digital camera images), along with the average corneal thickness (from pachymetry readings of the central and peripheral cornea). Our previous work has indicated that using an average corneal thickness leads to a ~2% change in predicted corneal behavior,[31] and it was therefore deemed an acceptable modeling simplification.

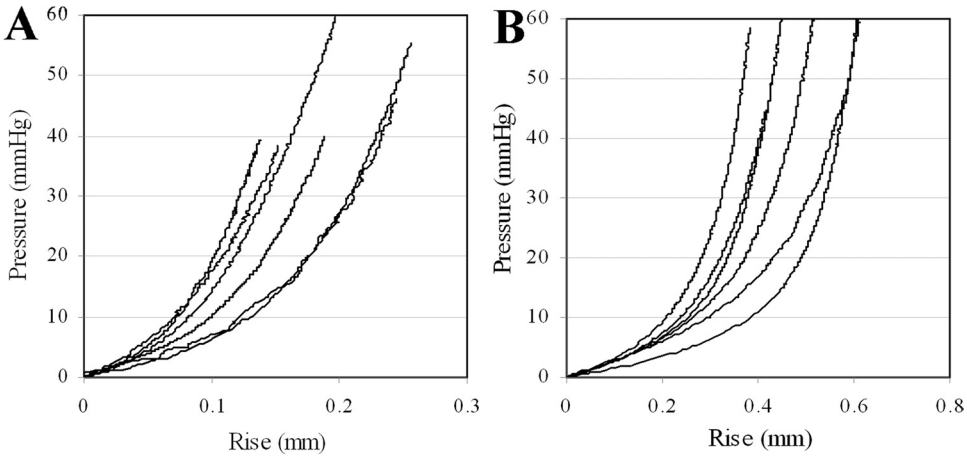

FIGURE 2. Trephinate inflation behavior of (**A**) six normal and (**B**) six RGE chicken corneas. Measured linear displacement of corneal apex (Rise) is plotted as a function of applied posterior pressure recorded during the fourth loading cycle (i.e., after preconditioning).

A full mathematical derivation of the stress-strain calculation can be found in an earlier publication.[31] The apical rise, r, during inflation (recorded from the laser sensor) was defined as the linear displacement of the corneal apex position with respect to the initial value and is related to the applied posterior pressure, p, by the final equation:

$$r = \frac{pR^2}{2Et}(1-\nu)[1-e^{-\beta\eta}\cos(\beta\eta)], \quad (1)$$

where $\eta = \sin^{-1}(R_i/R)$, $\beta = (R/t)^{1/2}[3(1-\nu^2)]^{1/4}$, R is the corneal radius of curvature, t is the thickness, R_i is the average limbal radius, and ν is Poisson's ratio, taken as 0.49 because cornea is water-rich and may be considered an incompressible tissue.[28] Values of r and p were used to calculate the cornea's modulus of elasticity, E, at each measurement point during inflation and subsequently the corresponding strain, ε, defined as the ratio between the tissue's stretch and the initial dimension and given by

$$\varepsilon = \frac{pR}{2Et}(1-\nu)[1+\nu e^{-\beta\eta}\cos\beta\eta]. \quad (2)$$

The corresponding stress, σ, defined as the average internal force per unit area acting on the tissue's cross-section, is then given by

$$\sigma = \varepsilon E. \quad (3)$$

The calculation of equations 1–3 is repeated for every inflation measurement point to derive the stress-strain behavior of the tissue.

Second Harmonic Generation Multiphoton Microscopy

For in-plane visualization of corneal lamellae, corneas with scleral rim were excised from the fixed globes and 2 mm × 2 mm full-thickness tissue samples removed from the central cornea and the superior-nasal region of the peripheral cornea, the latter at a distance of ~1 mm from the sclera. These tissue pieces were then separated into anterior and posterior serial sections of 100–150 μm thickness using a sledge microtome (HM440E; Microm, Walldorf, Germany) before being slide-mounted for microscopy using 1:1 PBS/glycerol. Meanwhile, to facilitate through-plane inspection of lamellar interlacing, 100-μm–thick tissue cross sections perpendicular to the corneal plane were also prepared from the central cornea (along the superior-inferior meridian) and peripheral cornea (tangential to the limbus, ~1 mm from the sclera) by the same method.

Nonlinear laser-scanning multiphoton microscopy was performed using a commercial device (Zeiss LSM 510 META NLO; Carl Zeiss Ltd, Welwyn Garden City, UK). An ultrafast titanium-sapphire laser (Chameleon; Coherent, Ely, UK) operating at 800 nm and <140 fs/90 MHz pulses was used to generate SHG signals from fibrillar collagen[32,33] detected at 400 ± 10 nm in the forward direction (nondescanned detector). Serial optical sections were obtained using a 20 × /0.8 N.A. objective lens (Plan-Apochromat; Carl Zeiss, Ltd.) at either 1 or 2 μm z-focus intervals for in-plane or through-plane lamellar imaging, respectively. The resulting three-dimensional datasets were reconstructed and analyzed using a combination of software packages (LSM Image Examiner; Carl Zeiss, and ImageJ; developed by

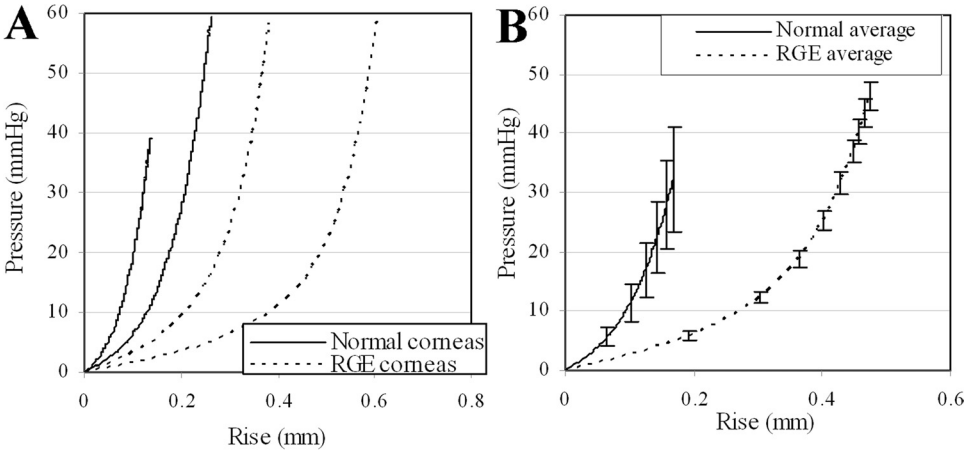

FIGURE 3. Comparison of inflation behavior between normal and RGE chicken corneas, showing for each group pressure-rise data for the (**A**) highest/lowest stiffness corneas and (**B**) the average of all corneas. Error bars, SD. From pressure-rise data RGE corneas appeared considerably less mechanically stiff.

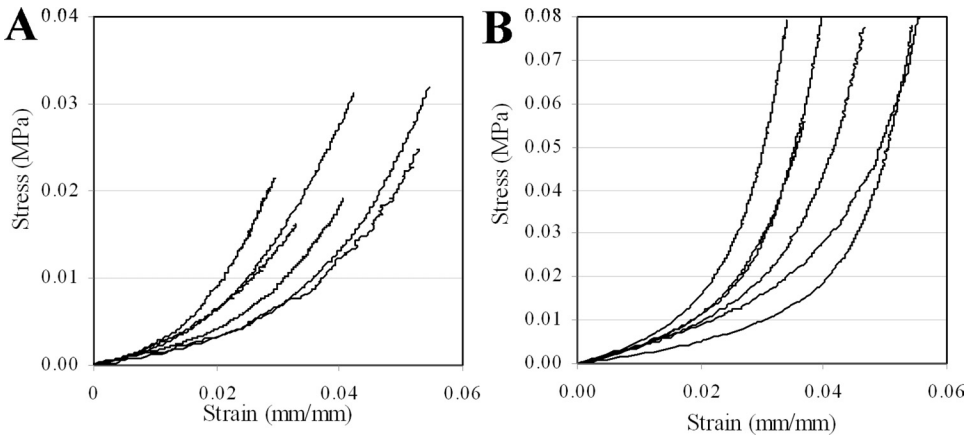

FIGURE 4. Stress-strain behavior of the **(A)** normal and **(B)** RGE chicken corneas, derived from pressure-rise data during the fourth cycle of inflation, using mathematical back-analysis that corrects for the effects of corneal geometry and thickness. Here stress represents the average internal force per unit area acting on the tissue's cross section, while strain is defined as the ratio between the tissue's stretch and initial dimension.

Wayne Rasband, National Institutes of Health, Bethesda, MD; available at http://rsb.info.nih.gov/ij/index.html).

RESULTS

Inflation Behavior

Results of apical rise versus applied posterior pressure are presented for normal and RGE corneas in Figure 2. All corneas exhibited an initial low stiffness phase up to a pressure of approximately 6–10 mm Hg, after which a gradual increase in stiffness was observed and continued to the end of the test. From pressure-deformation behavior RGE corneas appeared considerably less mechanically stiff than the normal controls (Fig. 3). For each specimen measurements of average corneal thickness (via pachymetry) and initial radius of curvature (via digital camera images) were used to derive stress-strain behavior from the pressure-rise data. A comprehensive treatment of the mathematical analysis used has been discussed previously.[31] The resulting stress-strain relationships for normal and RGE corneas are shown in Figure 4. Figure 5 compares the average stress-strain behavior of the two groups, and inspection of this figure reveals that, once tissue thickness and curvature was taken into account, the RGE corneas displayed increased material stiffness compared with age-matched controls. This difference was statistically significant at strains $\geq$0.035 mm/mm and became more pronounced with increasing strain (Fig. 5).

Inspection of Figures 3 and 5 confirms differences in both global inflation behavior and material stress-strain behavior of RGE corneas compared with age-matched normal controls. However, to gain a more direct measure of tissue stiffness, we also calculated and plotted the corneas' tangent modulus, $E_{tangent}$, as a function of applied stress (Fig. 6). The values of $E_{tangent}$ for the two groups were compared statistically using two-tailed *t*-tests over a range of applied stresses (and therefore posterior pressures), and the results are displayed alongside the average $E_{tangent}$ values in Table 1. A statistically significant ($P < 0.050$) 30–130% increase in $E_{tangent}$ was measured for RGE compared with normals over an average applied pressure range of 14.0–55.7 mm Hg, with significance marginally failing ($P = 0.051$) for the single measurement point at 20.8 mm Hg.

Collagen Microstructure

In-plane SHG signals from fibrillar collagen recorded from the central and peripheral normal avian cornea are presented in Figs. 7A, 7B and 7E, 7F, respectively. In the posterior-most quarter to third of the stroma, and extending from central cornea to limbus, we observed an orthogonal collagen mesh of fixed rotation (Figs. 7A and 7E). The remaining two-thirds to

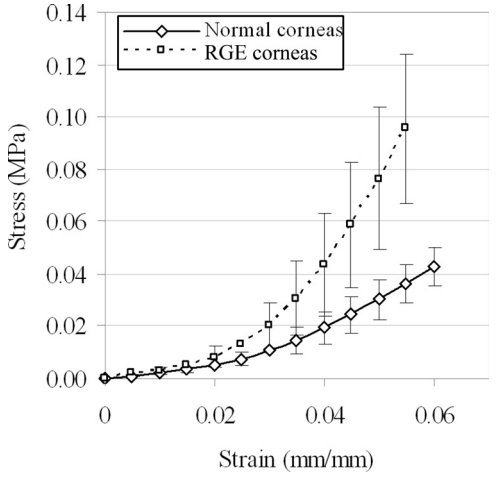

FIGURE 5. Average stress-strain behavior of normal and RGE chicken corneas. Error bars, SD. Once tissue thickness and geometry are accounted for, RGE corneas displayed significantly increased material stiffness compared with normal controls.

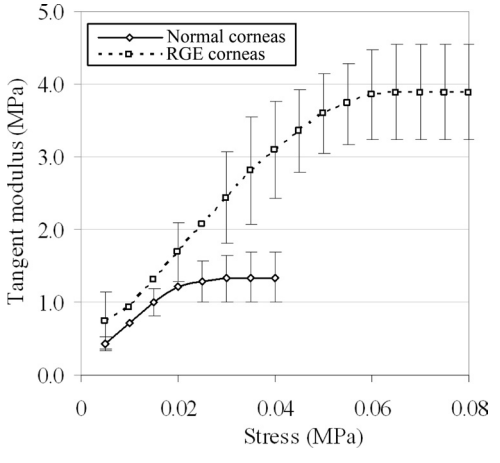

FIGURE 6. Tangent modulus ($E_{tangent}$), the gradient of a tangent line drawn at a given point on the stress-strain curve, plotted as a function of applied stress for normal and RGE chicken corneas under the fourth cycle of posterior pressure loading. Error bars, SD. A 30–130% increase in $E_{tangent}$, commonly considered a direct measure of tissue stiffness, is observed in RGE corneas compared with controls.

TABLE 1. Statistical Comparison of $E_{tangent}$ between Normal and RGE Corneas over a Range of Applied Posterior Pressures

Average Applied Pressure (mm Hg)	Average $E_{tangent}$ (MPa ± SD)		Difference ($E_{tangent}$)	*P*
	Normal	RGE		
7.1	0.44 ± 0.08	0.74 ± 0.41	70.1%	0.098
14.0	**0.72 ± 0.13**	**0.94 ± 0.18**	**29.8%**	**0.038**
20.8	**1.01 ± 0.19**	**1.31 ± 0.29**	**30.2%**	**0.051**
27.6	1.21 ± 0.27	1.69 ± 0.40	39.6%	0.033
34.3	1.29 ± 0.29	2.06 ± 0.52	60.0%	0.008
41.2	1.33 ± 0.32	2.44 ± 0.63	83.8%	0.002
48.9	1.34 ± 0.35	2.81 ± 0.74	109.5%	0.001
55.7	1.34 ± 0.35	3.09 ± 0.66	130.1%	0.000

Values were computed as the average of all specimens for a given pressure. Boldface denotes the physiological IOP range.

three-fourths of the stroma exhibited fibrous structures that followed more curved paths (Fig. 7B), in peripheral regions forming fan-like patterns (Fig. 7F), yet still retaining a lattice-like arrangement with 90° cross-angles. This superficial latticework was observed to rotate anticlockwise by 1° for every micron traversed in the posterior-anterior direction throughout the central (Fig. 8) and peripheral cornea.

The central cornea of RGE mutants appeared similar to that of normal birds (Figs. 7C, 7D). However fibrous structures in the peripheral anterior RGE cornea tended to follow straighter paths than in wild-type specimens, rendering the superficial lattice considerably less fanlike in appearance (Fig. 7H). To confirm that this difference was representative of the tissue as a whole, we performed tilings of *z*-stacks over the peripheral anterior sections (Figs. 9 and 10). The successive 1° per μm rotation of the superficial lattice observed in normal corneas was retained in mutants.

Through-plane SHG images from the normal and RGE cornea are shown in Figure 11. The posterior stroma of normal and RGE birds was observed to lie in well-defined stacked layers parallel to the corneal surface (Figs. 11A, 11C, 11E, 11G). In contrast, the anterior stroma appeared considerably more interwoven, with a large number of collagen fibril bundles running in the anterior-posterior direction, connecting adjacent layers (Figs. 11B, 11D, 11F, 11H). We observed no obvious differences in the degree or pattern of through-plane collagen interlacing between normal and RGE corneas.

DISCUSSION

In this article we have shown that the chicken cornea behaves as a nonlinear hyperelastic material with initial low-stiffness and final high-stiffness phases (Figs. 2–5). This behavior is typical of collagenous biological tissues, and similar results are well documented from corneal inflation tests using mammalian tissue.[28,34,35] To our knowledge the present work is the first published corneal inflation study to include avian data, although similar stress-strain behavior in chicken cornea has been noted from uniaxial strip tests.[36] The transition from low to high stiffness that we observe under inflation likely relates to the straightening of relaxed fibrils, allowing them to more effectively take up the membrane stresses imposed by posterior corneal pressure.[34]

An important result of the present study was the considerable difference in material stress-strain behavior observed between normal chicken corneas and those affected by the RGE mutation (Figs. 5, 6), with the RGE group displaying a statistically significant ($P \leq 0.05$) 30–130% increase in tangent modulus over a range of applied pressures in the region of, and well beyond, those experienced physiologically by these animals[22,23,37] (Table 1). It is our hypothesis that the difference in material behavior between RGE and normal corneas is microstructure related. In a previous paper we used x-ray scattering to show that the preferential collagen orientation is altered in the peripheral corneal region of RGE homozygotes. We noted that affected corneas did not feature a clear tangential disposi-

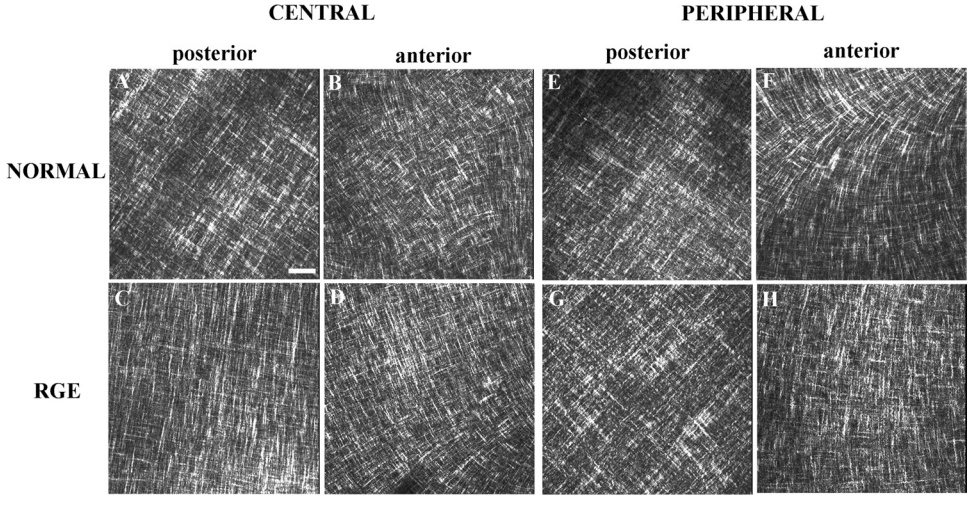

FIGURE 7. In-plane SHG collagen signals from the normal and RGE chicken cornea at stromal depths of 225 μm (posterior) and 50 μm (anterior). Bar, 50 μm. An orthogonal collagen straight latticework is evident in the posterior stroma (**A**, **C**, **E**, **G**). These structures appear wavier in the anterior stroma, while still retaining their lattice-like arrangement with 90° cross-angles (**B**, **D**). The characteristic fanlike structures in the peripheral anterior stroma of the normal cornea (**F**) are notably absent in RGE (**H**).

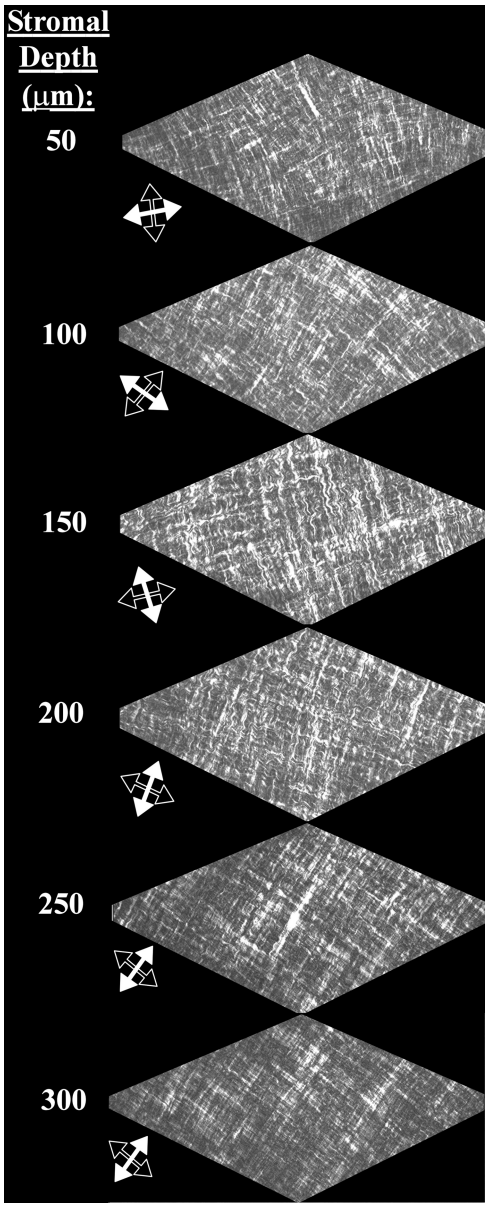

FIGURE 8. Depth profile of in-plane SHG collagen signals from the central normal chicken cornea. Throughout the most superficial ~3/4 of the stromal depth a 1°/μm anticlockwise rotation of fibrils is evident as the tissue is traversed in the posterior-anterior direction. In contrast, the orientation of lamellae in the deepest ~1/4 of the stroma is fixed. *Arrows* denote the directions of the two principal, mutually orthogonal, fibril populations at each depth.

tion of collagen circumscribing the central cornea as did normal birds, with mutants instead displaying a preponderance of orthogonally aligned collagen over the entire cornea.[24,25] Therefore to further test our hypothesis and gain a more visual, and moreover depth-resolved, insight into microstructural changes in RGE, we initiated a multiphoton microscopy investigation.

Using the SHG signal from collagen fibril bundles we were able to infer information about the in-plane disposition of corneal lamellae (Figs. 7–10). Our observation that the normal chicken cornea is organized into a posterior orthogonal system of fixed rotation, and an anterior system of successively rotated layers of more curved appearance aligns well with the established view of the mature avian stroma based on studies of

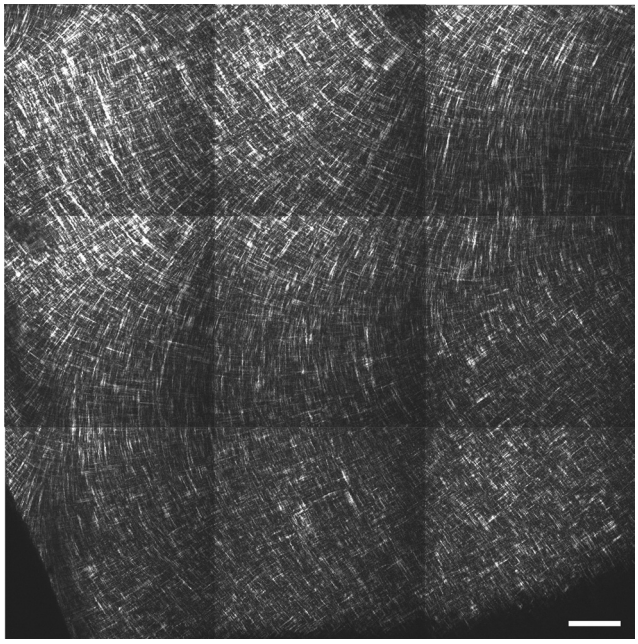

FIGURE 9. In-plane SHG collagen signals from a 1.2 mm × 1.2 mm peripheral region of the anterior normal chicken cornea with depth, 50 μm. Bar, 100 μm. The fanlike arrangement of anterior lamellae, characteristic of the chicken eye, dominates the peripheral cornea.

adult[38] and late-stage embryonic[39–41] tissue. We and others[40,41] have determined the total rotation of anterior stromal layers in the chick to be of the order of 200°, and we may reconcile this with our previous x-ray results[24] if we consider that the latter technique yields data that average the stromal thickness. Presumably, then, the ~200° rotation of layers in the central cornea (Fig. 8) is close enough to 180° to produce

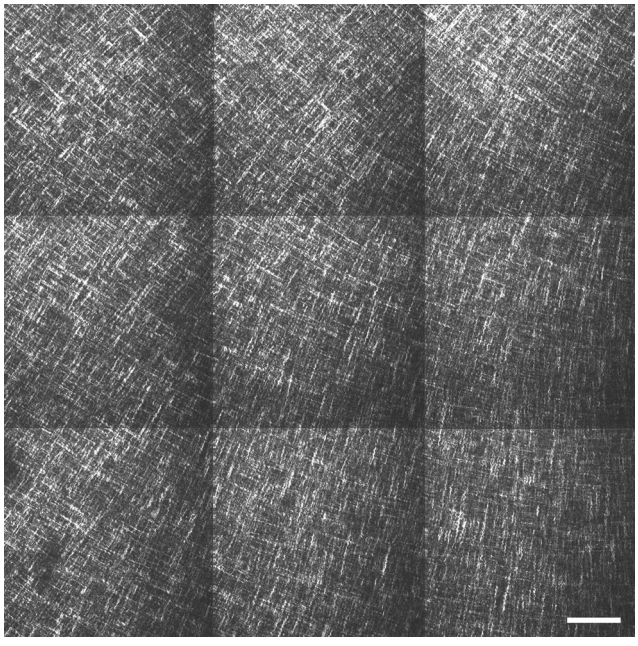

FIGURE 10. In-plane SHG collagen signals from a 1.2 mm × 1.2 mm peripheral region of the anterior RGE chicken cornea at a stromal depth of 50 μm. Bar, 100 μm. Anterior collagen structures in peripheral regions of mutant corneas appear straighter than those of the normal cornea.

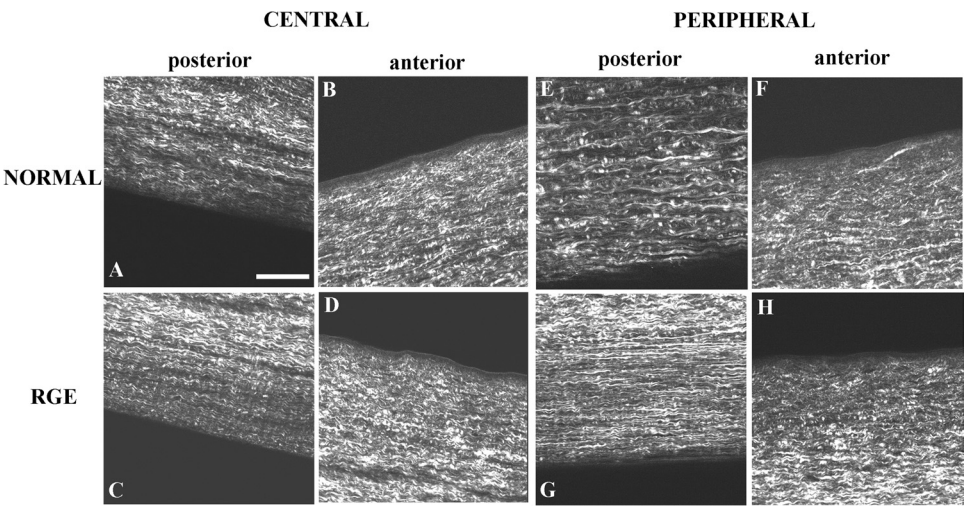

FIGURE 11. Through-plane SHG collagen signals from the normal and RGE chicken cornea. Bar, 50 μm. In the posterior stroma collagen lies in well-defined stacked layers parallel to the corneal plane (**A**, **C**, **E**, **G**). In contrast, the anterior stroma appears a more interwoven structure, with collagen fibril bundles connecting adjacent layers (**B**, **D**, **F**, **H**). No difference in the pattern of through-plane collagen arrangement was observed between normal and RGE tissue.

an x-ray signal that "averages out" over the anterior system, yielding a net orthogonal signal from the underlying fixed posterior lattice. In the present study we did not observe any discrete structures in the corneal periphery to account for the predominantly tangential collagen arrangement indicated by x-ray scattering. However, we propose that the superposition of more curved or fan-like anterior layers (Figs. 7F and 9) must somehow produce an overall preponderance of tangential collagen in the periphery, masking the orthogonal x-ray signal from the deep stroma. This scheme would also be consistent with documented evidence that surface split lines in the hen cornea form predominantly parallel to the limbus in the tissue periphery[38] and with subsequent observations from dissection of the dried specimens that supported the presence of circular lamellae.[38] Accordingly, we further contend that an alteration in the fanlike arrangement of individual anterior layers in the corneal periphery of RGE mutants, in favor of straighter structures more akin to the central anterior cornea (Figs. 7H and 10), could explain both the lack of a tangential x-ray collagen signal previously noted and the material alteration of the tissue described here.

How can peripheral changes in collagen lamellar organization be reconciled with the changes in corneal mechanical stiffness observed during inflation testing? In addressing this question it is relevant to review current understanding of corneal biomechanics. The mechanical stiffness of the cornea, or its resistance to deformation, is influenced by its geometric and material parameters.[42] In the case of a cornea inflated by posterior pressure, the dominant geometric parameters are the thickness and curvature.[31] With thinner and flatter corneas the mechanical stiffness is reduced, leading to more compliance and hence increased deformation. In contrast, a corneal tissue with higher tangent modulus, commonly considered a measure of material stiffness, is expected to have higher mechanical stiffness and hence reduced deformation. With this understanding in mind, it is now possible to consider the geometric and material differences between normal and RGE corneas. First, because RGE corneas have considerably flatter curvature (or larger radius),[22,23] they would be expected to have a lower mechanical stiffness and hence experience larger deformations under pressure elevation. With respect to the present study this effect would be further compounded by the reduced thickness of the RGE tissue indicated by our pachymetric measurements. However, RGE corneas have also exhibited continuous meridian stromal fibrils,[24,25] in contrast to normal tissue, which demonstrates a change in fiber orientation from meridian at the center to circumferential in the periphery.[24] This difference in structure is expected to make RGE tissue stiffer (i.e., have a higher tangent modulus) than normal corneal tissue (as shown in Fig. 6), because meridian fibrils are able take up the radial stresses imposed by posterior pressure more effectively than tangential fibrils.[34] It is therefore clear that, although the smaller thickness and flatter curvature decrease the RGE corneas' mechanical stiffness, their high-tangent modulus values have the opposite effect. It is also evident from the pressure-rise results of the inflation tests that the geometric differences have dominated the behavior comparisons and made RGE corneas less mechanically stiff overall than normal corneas (Fig. 3).

Before drawing general conclusions about corneal behavior from the present results, a number of factors should be taken into account. First, it should be noted that the architectures of the mature avian and mammalian stroma differ at a fundamental level,[14] likely as a legacy of contrasting developmental processes.[43,44] This may partly reflect biomechanical requirements, such as those imposed by the need for the avian cornea to accommodate.[45] Second, the trephinate inflation method used in our study involves the cornea and limbus but, in clamping the tissue outside the limbus, neglects the influence of the sclera. In doing this we inevitably compromise to some extent the natural load-bearing environment of the cornea because, under in vivo conditions, the sclera may be expected deform in response to IOP, thereby affecting the cornea.[31] Indeed, modeling studies have indicated that the biomechanical stability of the anterior eye is likely maintained by a precise rheological balance between the cornea, limbus, and sclera.[46–50] Moreover, the possible in vivo effects on the RGE cornea of both increased scleral size and the likely scleral restructuring implied by globe enlargement[22–25] cannot be assessed using trephinates. Third, a limitation of the mathematical shell analysis used to calculate stress-strain behavior is that it approximates the chicken cornea as a homogeneous, spherical structure,[26] whereas in reality it is both aspheric and, as we have shown in the current paper and previously[24,25] demonstrates variation in collagen fibril aligment as a function of corneal position and depth. Last, possible alterations in noncollagenous corneal matrix components, such as specific proteoglycan types and collagen cross-links have not been investigated in RGE.

Nevertheless the present study has enabled us, on a qualitative level, to investigate effectively the relationship between in vitro corneal material behavior and collagen fibril alignment. Importantly, the results suggest that changes in the preferential orientation of stromal lamellae may significantly affect the cornea's material stiffness and thereby its biomechanical response to IOP. The formulation of a mathematical relationship

with which to model the fibril alignment changes in RGE and their affect on the avian corneal modulus will rely on appropriate quantification of the microstructural alterations presented qualitatively here. Some quantification of fibril realignment in RGE has been achieved previously by x-ray scattering.[24,25] However x-ray data average the stromal thickness and the technique cannot, on its own, describe the full extent of the three-dimensional microstructural changes indicated by the present study. Finite-element models of the mammalian cornea that include fibril orientation data have already been produced[48,51–53] and have achieved some success in predicting corneal behavior[52,53] and its response to certain refractive surgeries.[48,51] The construction of a numerical model of the avian cornea is likely to prove even more challenging given the evidently unique and complex three-dimensional structure of the avian stroma. This will form the focus of our future research efforts.

Acknowledgments

The authors thank Graeme Robertson at the Roslin Institute for technical expertise. The Zeiss multiphoton laser scanning microscope is a Cardiff Institute of Tissue Engineering and Repair (CITER) facility.

References

1. Fatt I, Weissman B. Physiology of the Eye: *An Introduction to the Vegetative Functions.* 2nd ed. Boston: Butterworth-Heinmann; 1992.
2. Maurice DM. The structure and transparency of the cornea. *J Physiol.* 1957;136:263–286.
3. Meek KM. The cornea and sclera. In: Fratzl P, ed. *Collagen: Structure and Mechanics*. New York: Springer; 2008:359–396.
4. Meek KM. Corneal collagen—its role in maintaining corneal shape and transparency. *Biophys Rev.* 2009;1:83–93.
5. Boote C, Dennis S, Huang Y, Meek K. Lamellar orientation in human cornea in relation to mechanical properties. *J Struct Biol.* 2005;149:1–6.
6. Elsheikh A, Alhasso D. Mechanical anisotropy of porcine cornea and correlation with stromal microstructure. *Exp Eye Res.* 2009; 88:1084–1091.
7. Hjortdal JO. Regional elastic performance of the human cornea. *J Biomech.* 1996;29:931–942.
8. Li LY, Tighe B. The anisotropic material constitutive models for the human cornea. *J Struct Biol.* 2006;153:223–230.
9. Ruberti J, Zieske J, Trinkaus-Randall V. Corneal tissue replacement. In: Lanza R, Langer R, Vacanti J, eds. *Principles of Tissue Engineering*. New York: Elsevier/Academic Press; 2007.
10. Shin TJ, Vito RP, Johnson LW, McCarey BE. The distribution of strain in the human cornea. *J Biomech.* 1997;30:497–503.
11. Smolek MK, McCarey BE. Interlamellar adhesive strength in human eyebank corneas. *Invest Ophthalmol Vis Sci.* 1990;31:1087–1095.
12. Bron AJ. Editorial: The architecture of the corneal stroma. *Br J Ophthalmol.* 2001;85:379–383.
13. Muller LJ, Pels E, Vrensen GFJM. The specific architecture of the anterior stroma accounts for maintenance of corneal curvature. *Br J Ophthalmol.* 2001;85:437–443.
14. Polack FM. Morphology of the cornea. *A J Ophthalmol.* 1961;51: 179–184.
15. Elsheikh A, Ross S, Alhasso D, Rama P. Numerical study of the effect of corneal layered structure on ocular biomechanics. *Curr Eye Res.* 2009;34:26–35.
16. Gefen A, Shalom R, Elad D, Mandel Y. Biomechanical analysis of the keratoconic cornea. *J Mech Behav Biomed Mater.* 2009;2: 224–236.
17. Kerautret J, Colin J, Touboul D, Roberts C. Biomechanical characteristics of the ectatic cornea. *J Cataract Refract Surg.* 2008;34: 510–513.
18. Roy AS, Dupps WJ Jr. Effects of altered corneal stiffness on native and postoperative LASIK corneal biomechanical behavior: whole-eye finite element analysis. *J Refract Surg.* 2009;25:875–887.
19. Curtis PE, Baker JR, Curtis R, Johnston A. Impaired vision in chickens associated with retinal defects. *Vet Record.* 1987;120:113–114.
20. Curtis R, Baker JR, Curtis PE, Johnston A. An inherited retinopathy in commercial breeding chickens. *Avian Pathol.* 1988;17:87–99.
21. Tummala H, Ali M, Getty P, et al. Mutation in the guanine nucleotide-binding protein beta-3 causes retinal degeneration and embryonic mortality in chickens. *Invest Ophthalmol Vis Sci.* 2006; 47:4714–4718.
22. Inglehearn C, Morrice D, Lester D, et al. Genetic, ophthalmic, morphometric and histopathological analysis of the retinopathy globe enlarged (RGE) chicken. *Mol Vis.* 2003;9:295–300.
23. Montiani-Ferreira F, Li T, Kiupel M, et al. Clinical features of the retinopathy, globe enlarged (RGE) chick phenotype. *Vis Res.* 2003; 43:2009–2018.
24. Boote C, Hayes S, Jones S, et al. Collagen organization in the chicken cornea and structural alterations in the retinopathy, globe enlarged (RGE) phenotype—an X-ray diffraction study. *J Struct Biol.* 2008;161:1–8.
25. Boote C, Hayes S, Young RD, et al. Ultrastructural changes in the retinopathy, globe enlarged (RGE) chick cornea. *J Struct Biol.* 2009;166:195–204.
26. Elsheikh A, Wang D, Brown M, et al. Assessment of corneal biomechanical properties and their variation with age. *Curr Eye Res.* 2007;32:11–19.
27. Zeng Y, Yang J, Huang K, Lee Z, Lee X. A comparison of biomechanical properties between human and porcine cornea. *J Biomech.* 2001;34:533–537.
28. Bryant MR, McDonnell PJ. Constitutive laws for biomechanical modeling of refractive surgery. *J Biomech Eng.* 1996;118:473–481.
29. Carew EO, Barber JE, Vesely I. Role of preconditioning and recovery time in repeated testing of aortic valve tissues: validation through quasilinear viscoelastic theory. *Ann Biomed Eng.* 2000; 28:1093–1100.
30. Kothe AC. The effect of posture on intraocular pressure and pulsatile ocular blood flow in normal and glaucomatous eyes. *Surv Ophthalmol.* 1994;38:S191–197.
31. Anderson K, Elsheikh A, Newson T. Application of structural analysis to the mechanical behaviour of the cornea. *J R Soc Interface.* 2004;1:3–15.
32. Farid M, Morishige N, Lam L, et al. Detection of corneal fibrosis by imaging second harmonic-generated signals in rabbit corneas treated with mitomycin C after excimer laser surface ablation. *Invest Ophthalmol Vis Sci.* 2008;49:4377–4383.
33. Kamma-Lorger CS, Boote C, Hayes S, et al. Collagen and mature elastic fibre organisation as a function of depth in the human cornea and limbus. *J Struct Biol.* 2010;169:424–430.
34. Boyce BL, Grazier JM, Jones RE, Nguyen TD. Full-field deformation of bovine cornea under constrained inflation conditions. *Biomaterials.* 2008;4:4.
35. Elsheikh A, Alhasso D, Rama P. Biomechanical properties of human and porcine corneas. *Exp Eye Res.* 2008;86:783–790.
36. Loewenstein MA, Bettelheim FA. Comparative rheology of cornea. *Comp Biochem Physiol A—Physiol.* 1976;55:363–365.
37. Prashar A, Guggenheim JA, Erichsen JT, Hocking P, Morgan JE. Measurement of intraocular pressure (IOP) in chickens using a rebound tonometer: quantitative evaluation of variance due to position inaccuracies. *Exp Eye Res.* 2007;85:563–571.
38. Lucio A, Smith RL. Architecture of the corneal stroma of the hen. *Acta Anatomica.* 1984;120:196–201.
39. Coulombre AJ. Problems in corneal morphogenesis. *Advan Morphogenesis.* 1965;4:81–109.
40. Svoboda K, Petroll WM, Jester JV. Second harmonic signal analysis of whole embryonic avian corneas. *Microscop Microanal.* 2007; 13(S02):1550–1551.
41. Trelstad RL, Coulombre AJ. Morphogenesis of the collagenous stroma in the chick cornea. *J Cell Biol.* 1971;50:840–858.
42. Liu J, Roberts CJ. Influence of corneal biomechanical properties on intraocular pressure measurement: quantitative analysis. *J Cataract Refract Surg.* 2005;31:146–155.
43. Cintron C, Covington H, Kublin CL. Morphogenesis of rabbit corneal stroma. *Invest Ophthalmol Vis Sci.* 1983;24:543–556.

44. Hay ED, Revel JP. Fine structure of the developing avian cornea. *Monogr Dev Biol.* 1969;1:1–144.
45. Glasser A, Troilo D, Howland HC. The mechanism of corneal accommodation in chicks. *Vis Res.* 1994;34:1549–1566.
46. Asejczyk-Widlicka M, Srodka DW, Kasprzak H, Pierscionek BK. Modelling the elastic properties of the anterior eye and their contribution to maintenance of image quality: the role of the limbus. *Eye (Lond).* 2007;21:1087–1094.
47. Pandolfi A, Manganiello F. A model for the human cornea: constitutive formulation and numerical analysis. *Biomech Model Mechanobiol.* 2006;5:237–246.
48. Pinsky PM, Van der Heide D, Chernyak D. Computational modeling of mechanical anisotropy in the cornea and sclera. *J Cataract Refract Surg.* 2005;31:136–145.
49. Srodka W, Iskander DR. Optically inspired biomechanical model of the human eyeball. *J Biomed Opt.* 2008;13:044034.
50. Srodka W, Pierscionek BK. Effect of material properties of the eyeball coat on optical image stability. *J Biomed Opt.* 2008;13:054013.
51. Lanchares E, Calvo B, Cristóbal JA, Doblaré M. Finite element simulation of arcuates for astigmatism correction. *J Biomech.* 2008;41:797–805.
52. Nguyen TD, Jones RE, Boyce BL. A nonlinear anisotropic viscoelastic model for the tensile behavior of the corneal stroma. *J Biomech Eng.* 2008;130:041020.
53. Pandolfi A, Holzapfel GA. Three-dimensional modeling and computational analysis of the human cornea considering distributed collagen fibril orientations. *J Biomech Eng.* 2008;130:061006.